Analysis and Design of a Single-Switch Forward-Flyback Two-Channel LED Driver With Resonant-Blocking Capacitor

Jong-Woo Kim, *Student Member, IEEE*, Jung-Pil Moon, *Student Member, IEEE*, and Gun-Woo Moon, *Member, IEEE*

***Abstract*—In order to balance the light-emitting-diode (LED) current in each channel, many active and passive methods have been investigated. Among the various methods, the passive method using the LLC converter with a blocking capacitor or flyback converter with a current-sharing transformer (CST) in the secondary side is one of the simplest methods because it does not use any active component. However, the LLC driver requires two main switches and external resonant inductor to obtain a wide output voltage range. Also, flyback with a CST requires an additional magnetic component for CST and high-voltage rated diodes, resulting in the limitation of the cost and system volume. In this paper, a single-switch forward-flyback driver for a two-channel LED is proposed. The most powerful advantage of the proposed driver is the cost effectiveness, since it eliminates additional magnetic component. Furthermore, due to the reduced-voltage stress on rectifier diodes compared to the flyback driver, the proposed driver achieves a higher efficiency. The prototype of the 150–100-V/0.3-A two-channel LED verifies the effectiveness of this paper.**

***Index Terms*—Blocking capacitor, forward-flyback converter, passive current balancing, two-channel LED driver.**

I. Introduction

NOWADAYS, the light-emitting-diode (LED) market has been rapidly growing. From low-power applications such as a flashlight to midpower applications such as a streetlight, the LED is replacing the other light sources because of its long lifetime, high efficiency, and its eco-friendly characteristics [1], [2].

In the midpower applications, a two-stage structure, which is composed of a boost power factor correction (PFC) and an isolated dc/dc converter stage, is widely used. The boost PFC provides a high power factor and a low total harmonic distortion, and the dc/dc stage regulates the LED current to control the luminance. Because the current of LED determines its luminance, a series-connected LED string is widely used in the midpower applications. However, too many LEDs in series result in a high output voltage of the dc/dc converter, which burdens the output capacitor. Furthermore, the reliability of the driver also can be reduced because the light will be turned OFF when only one module is broken [3]. For these reasons, LED strings are connected in parallel, and a two-channel structure is widely used in near 100-W applications, as shown in Fig 1. In the two-channel structure, the current in each channel must be balanced because the LED has the negative temperature coefficient of the forward voltage drop. Therefore, it is required for the two channel LED driver to have not only current balancing characteristic, but also the wide output voltage range capability.

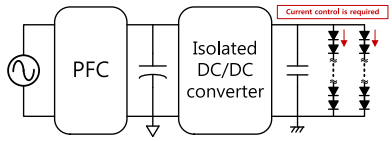

Fig. 1. Structure of a two-channel LED driver.

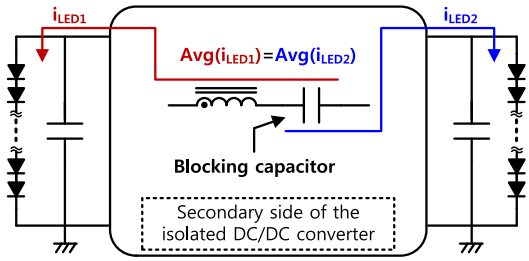

Fig. 2. Capacitive current balancing method for a two-channel LED driver with a blocking capacitor.

Among many current balancing techniques [3]–[14], the passive current balancing methods have been investigated as a solution for many components of the active current balancing methods. The passive balancing methods can be subdivided into the capacitive and inductive balancing.

The key concept of the capacitive current balancing methods is the use of blocking capacitor, as shown in Fig. 2. A series-connected blocking capacitor in the secondary side of the transformer balances the current of two LED strings. By the charge conservation, the average current flows through the two LED strings ($\mathrm{Avg}(i_{\mathrm{LED1}})$ and $\mathrm{Avg}(i_{\mathrm{LED2}})$ in Fig. 2) are naturally balanced without the active components [9], [11]–[14]. The capacitive method is very cost effective in that it uses a small number of components. In the primary side of the passive current balancing drivers, a current-source-type inverter is required in order to use the charge balance of the blocking capacitor. The LLC converter is widely used because of its

Manuscript received December 1, 2014; revised March 15, 2015; accepted April 25, 2015. Date of publication May 12, 2015; date of current version November 16, 2015. This work was supported by the National Research Foundation of Korea supported by the Korea government (MSIP) under Grant 2010-0028680. Recommended for publication by Associate Editor S. Y. Hui.

J.-W. Kim and G.-W. Moon are with the Department of Electrical Engineering, Korea Advanced Institute of Science and Technology, Daejeon 305-701, Korea (e-mail: jongwoo.kim@kaist.ac.kr; gwmoon@ee.kaist.ac.kr).

J.-P. Moon is with the Department of Electrical Engineering, Korea Advanced Institute of Science and Technology, Daejeon 305-701, Korea and also with Samsung Electronics, Suwon 443-742, Korea (e-mail: Jungpil.moon@samsung.com).

Color versions of one or more of the figures in this paper are available online at http://ieeexplore.ieee.org.

Digital Object Identifier 10.1109/TPEL.2015.2432458

zero-voltage-switching characteristics. However, the LLC converter requires two main switches and the additional resonant inductor to obtain wide output voltage range. Therefore, the passive current balancing drivers that use the LLC converter have a limitation in their system volume and cost.

The inductive methods [3], [4] use a current-sharing transformer (CST) in series with each LED string so that the current of each string is automatically balanced. Especially, a flyback converter can be used in the two-channel structure [3]. This method can be a cost-effective solution for the two-channel driver because the flyback converter is well known for low cost and wide output voltage capability. However, it requires additional magnetic component and the CST should be carefully designed in order to prevent the current in each string from being unbalanced. Furthermore, the voltage stress on the rectifier diodes is too high because of a complicated resonance between the CST and the rectifier diodes during the reset of the CST. Therefore, the cost problem, core loss, and large conduction losses are unavoidable with the structure because the CST causes core loss due to the voltage difference between two channels, and high-voltage-rated rectifier diodes have a high forward voltage drop.

In this paper, a single-switch isolated driver for two-channel LED strings is proposed. First, by using an on-time-controlled forward-flyback inverter in the primary side, the proposed driver obtains a wide output voltage range. Because the proposed driver can use a small leakage inductor as the resonant component, the additional external inductor can be eliminated. Second, the proposed driver has clamped-voltage stress on the rectifier diodes so that the low-voltage-rated rectifier diodes can be used. The most powerful advantage of the proposed driver is the cost effectiveness, since it uses only one main switch and the main transformer, without additional magnetic components. Furthermore, voltage stress of the secondary-side rectifier diodes is clamped, so that it is possible to obtain in a further reduced conduction loss compared to the flyback driver.

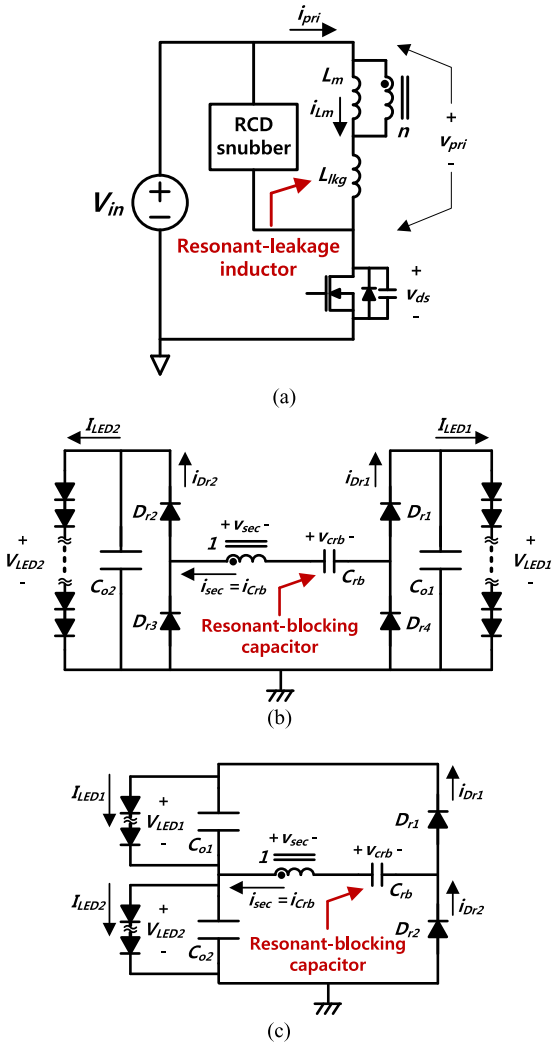

Fig. 3. Proposed two-channel LED driver. (a) Primary side. (b) Secondary side with full-bridge-type rectifier. (c) Secondary side with voltage-doubler-type rectifier.

II. Proposed Driver

Figs. 3 and 4 show the proposed driver and its key waveforms. As shown in Fig. 3(a), a single-switch inverter is used in the primary side of the proposed driver. The proposed driver is controlled by the on time of the main switch. In order to reduce the switching loss of the primary-side inverter, the proposed driver operates with the valley switching technique, and the magnetizing inductor of the main transformer operates in the boundary conduction mode (BCM). Fig. 3(b) and (c) illustrates the secondary side of the proposed driver with a full-bridge and voltage-double-type rectifier, respectively. The only difference between two rectifiers is only voltage stress on rectifier diodes. For simplicity, this paper deals with the below resonant region of the proposed driver.

A. Operational Mode Analysis

Mode 1 ($t_0 - t_1$): The main switch is turned ON when the voltage across the switch (v_{ds}) is minimum. The resonant current between the leakage inductor of the transformer ($L_{\rm lkg}$) and the resonant-blocking capacitor (C_{rb}) is transferred to the output capacitor C_{o2}. The effective resonant factors during mode 1 are $L_{\rm lkg}/n^2$ and C_{rb} because $L_{\rm lkg}$ is reflected to the secondary side of the transformer. The voltage across the resonant-blocking capacitor (v_{crb}) decreases with the resonance. The voltage on the primary side of the transformer ($v_{\rm pri}$) is equal to the input voltage ($V_{\rm in}$). Assuming that the magnetizing inductor (L_m) has a much larger inductance than $L_{\rm lkg}$, the current of magnetizing inductor (i_{Lm}) increases with the slope of $V_{\rm in}/L_m$. The current difference between $i_{\rm pri}$ and i_{Lm} is transferred to the secondary side through D_{r2} and D_{r4}. The powering to C_{o2} ends when the primary-side current of the transformer ($i_{\rm pri}$) becomes equal to i_{Lm}. The secondary-side current of the transformer ($i_{\rm sec}$) becomes zero. The amount of energy transferred to C_{o2} during this mode is equal to that of the energy stored in C_{rb} when the main switch is turned OFF.

The duration of mode 1 is approximately a half of the resonant period $\pi\sqrt{L_{\rm lkg}C_{rb}}/n$, when the proposed driver operates near the resonant point.

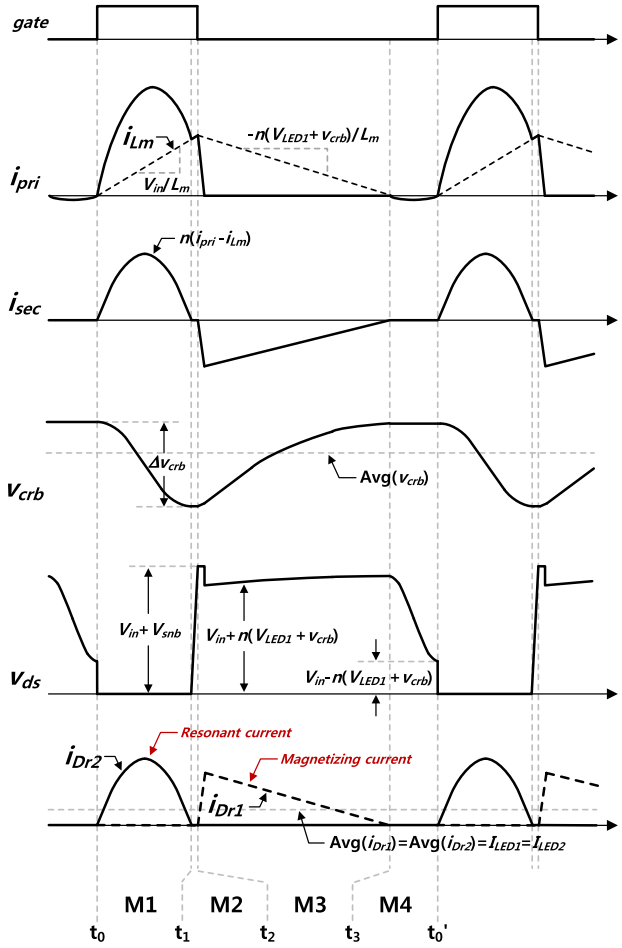

Fig. 4. Key waveforms of the proposed LED driver.

Mode 2 ($t_1 - t_2$): The main switch is still turned ON and i_{pri} increases linearly. Mode 2 ends when the main switch is turned OFF.

Mode 3 ($t_2 - t_3$): After the main switch is turned OFF, i_{pri} is reset by the RCD snubber and the energy stored in L_m is transferred to series-connected C_{rb} and C_{o1} through D_{r1} and D_{r3}. The voltage across L_m is $-n(V_{\mathrm{LED1}} + v_{crb})$. The voltage stress of the main switch becomes $V_{\mathrm{in}} + n(V_{\mathrm{LED1}} + v_{crb})$. i_{Lm} and $|i_{\mathrm{sec}}|$ decreases linearly. v_{crb} is increased by i_{sec}. During this mode, the amount of energy transferred by L_m should be equal to the amount of energy consumed at the series-connected C_{rb} and C_{o1}.

Mode 4($t_3 - t_0'$): After i_{Lm} becomes zero, v_{ds} decreases due to the resonance between the output capacitance of the main switch and $L_m + L_{\mathrm{lkg}}$. The main switch is turned ON when v_{ds} is the minimum.

When the proposed driver operates in an above resonant region, only mode 2 is eliminated because the main switch is turned OFF before the resonance between L_{lkg} and C_{rb} ends.

B. Steady-State Characteristics

In order to avoid complexity, it is assumed that the proposed driver operates at the resonant point, and the delayed switching period due to the valley switching is ignored, as shown in Fig. 5.

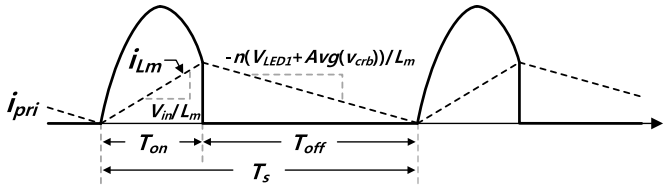

Fig. 5. Simplified primary current of the proposed driver.

The average value of v_{crb} ($\mathrm{Avg}(v_{crb})$) can be approximately-obtained applying the volt–sec balance at the secondary side of the transformer as follows:

$$\int_0^{T_{on}} \left[V_{\mathrm{LED2}} - v_{crb}\left(t\right)\right] dt = \int_{T_{on}}^{T_s} \left[V_{\mathrm{LED1}} + v_{crb}\left(t\right)\right] dt \tag{1}$$

$$T_{\mathrm{on}} V_{\mathrm{LED2}} - T_{\mathrm{off}} V_{\mathrm{LED1}} = \left(T_{\mathrm{on}} + T_{\mathrm{off}}\right) \mathrm{Avg}\left(v_{crb}\right) \tag{2}$$

$$T_{\mathrm{on}} \left[V_{\mathrm{LED2}} - \mathrm{Avg}\left(v_{crb}\right)\right] = T_{\mathrm{off}} \left[V_{\mathrm{LED1}} + \mathrm{Avg}\left(v_{crb}\right)\right] \tag{3}$$

where $T_s = T_{\mathrm{on}} + T_{\mathrm{off}}$ and $\mathrm{Avg}\left(v_{crb}\right) = \int_0^{T_s} v_{crb}\left(t\right) dt / T_s$.

Assuming that the magnetizing inductor (L_m) has a much larger inductance than L_{lkg}, the voltage across L_m becomes V_{in} when the main switch is turned ON. Then, the volt–sec balance on L_m can also be obtained as follows:

$$T_{\mathrm{on}} V_{\mathrm{in}} = T_{\mathrm{off}}\, n \left[V_{\mathrm{LED1}} + \mathrm{Avg}(v_{crb})\right]. \tag{4}$$

Combining (2) and (3) leads to the explicit form of $\mathrm{Avg}(v_{crb})$ can be obtained as follows:

$$\mathrm{Avg}(v_{crb}) = -\frac{V_{\mathrm{in}}}{n} + V_{\mathrm{LED2}}. \tag{5}$$

From (5), one interesting thing can be found that the voltage across C_{rb} is independent on V_{LED1}. V_{in}, n, and V_{LED2} determine $\mathrm{Avg}(v_{crb})$. The maximum $\mathrm{Avg}(v_{crb})$ occurs when $V_{\mathrm{LED2}} = 0$.

The ripple voltage of $C_{rb}(\Delta v_{crb})$ can be obtained by applying charge balance on C_{o1} as follows:

$$\Delta v_{crb} = I_{\mathrm{LED2}} T_s / C_{rb}. \tag{6}$$

The switching period T_s can be obtained from (4) and (6) as follows:

$$T_s = T_{\mathrm{on}} + T_{\mathrm{off}} = T_{\mathrm{on}} \frac{n(V_{\mathrm{LED1}} + V_{\mathrm{LED2}})/V_{\mathrm{in}}}{n(V_{\mathrm{LED1}} + V_{\mathrm{LED2}})/V_{\mathrm{in}} - 1}. \tag{7}$$

Actually, the switching period of the proposed driver has additional components, due to the resonance for valley switching. Exactly, the switching period would be $T_{\mathrm{on}} + T_{\mathrm{off}} + T_{\mathrm{res}}$, where T_{res} represents the resonant period for valley switching. Because T_{res} is constant, the half of the resonant period between L_m and output capacitor of the main switch, the minimum switching period cannot be smaller than T_{res}. However, in this paper, the effect of T_{res} is omitted for a simple design procedure.

Now, the energy conservation mentioned in mode 3 can provide the required T_{on} according to V_{LED1} and V_{LED2}. Fig. 6(a) shows the equivalent power delivery model of the proposed driver. The average current consumed at C_{o1} is I_{LED1},

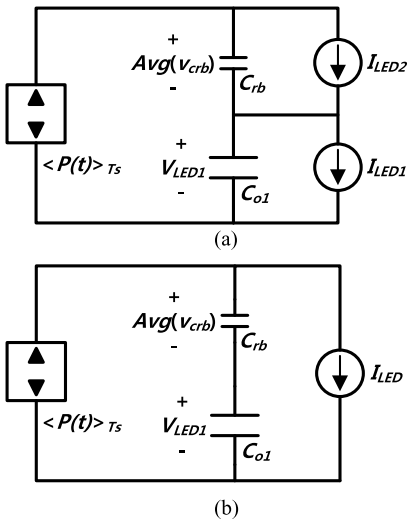

Fig. 6. Equivalent power delivery models of the proposed driver (a) focused on the energy stored in L_m and (b) a simplified form when $I_{\mathrm{LED}1} = I_{\mathrm{LED}2} = I_{\mathrm{LED}}$.

and the average current consumed at C_{rb} is $I_{\mathrm{LED}2}$. The average power delivered by L_m during T_s ($\langle P(t)\rangle_{Ts}$) is 0.5 $L_m(V_{\mathrm{in}}T_{\mathrm{on}}/L_m)^2/T_s$. When $I_{\mathrm{LED}2} = I_{\mathrm{LED}1} = I_{\mathrm{LED}}$ due to the charge balance on C_{rb}, the model can be simplified, as shown in Fig. 6(b). Therefore, the power consumed at C_{o1} and C_{rb} can be obtained as $(V_{\mathrm{LED}1} + \mathrm{Avg}(v_{crb}))I_{\mathrm{LED}}$. The energy delivered by L_m during T_s ($\langle P(t)\rangle_{Ts}T_s$) must be equal to the energy consumed at C_{o1} and C_{rb}, and this condition leads to the following:

$$0.5\,L_m T_s (V_{\mathrm{in}}T_{\mathrm{on}}/L_m)^2/T_s = (V_{\mathrm{LED}1} + \mathrm{Avg}(v_{crb}))I_{\mathrm{LED}}T_s. \tag{8}$$

Combining (6)–(9) leads to the required T_{on} according to $V_{\mathrm{LED}1}$ and $V_{\mathrm{LED}2}$ as follows:

$$(V_{\mathrm{LED}1} + V_{\mathrm{LED}2})/V_{\mathrm{in}} = V_{\mathrm{in}}T_{\mathrm{on}}/2L_m I_{\mathrm{LED}} \tag{9}$$

$$T_{\mathrm{on}} = 2L_m I_{\mathrm{LED}}(V_{\mathrm{LED}1} + V_{\mathrm{LED}2})/V_{\mathrm{in}}^2. \tag{10}$$

It can be noted that *n* is eliminated during the rearranging, and only T_{on} determines the output voltage of LED strings. Larger the T_{on}, larger the $V_{\mathrm{LED}1} + V_{\mathrm{LED}2}$. Similar with the conventional BCM flyback converter, the output voltage of the proposed driver only depends on T_{on}.

C. Control-to-Output Small-Signal Modeling

In order to ensure stability of the system, the control-to-output transfer function ($G_{vc}(s)$) should be investigated. In the proposed driver, $G_{vc}(s)$ can be obtained in a similar way with a conventional flyback converter in BCM [15], excepting that C_{rb} is series connected with the output capacitors. In order to obtain $G_{vc}(s)$, the average current flowing through D_{r1} and D_{r2} ($\langle i_{Dr1}\rangle$ and $\langle i_{Dr2}\rangle$) should be obtained according to the on-time variation. To avoid complexity, it is assumed that $\langle i_{Dr1}\rangle$ and $\langle i_{Dr2}\rangle$ become naturally equal because of the charge conservation of C_{rb}. From the previous mode analysis, the amount of charge transferred to C_{o2} during T_{on} is equal to that of the energy stored in C_{rb} during T_{off}. Also, the amount of charge transferred to C_{o1} during T_{off} is equal to the amount of charge stored in C_{rb}

$$\langle i_{Dr1}\rangle = \langle i_{Dr2}\rangle = \langle i_{Dr}\rangle. \tag{11}$$

Although the proposed driver operates in a transient state, this condition is still satisfied because the response of the resonant tank is very fast. The resonant frequency of the proposed driver is close to the switching frequency, so that its response can be neglected assuming that the cutoff frequency of the system is usually located lower than 1/10 of the switching frequency.

From Figs. 5 and 6, $\langle i_{Dr1}\rangle$ can be obtained as follows:

$$\langle i_{Dr}\rangle = \frac{Q_{Dr1}}{T_s} = \frac{V_{in}^2 T_{on}}{2L_m(V_{\mathrm{LED}1} + V_{\mathrm{LED}2})}. \tag{12}$$

In order to obtain control-to-output transfer function, $\partial\langle i_{Dr1}\rangle/\partial T_{\mathrm{on}}$ and $\partial\langle i_{Dr1}\rangle/\partial(V_{\mathrm{LED}1})$ should be considered as follows:

$$\frac{\partial\langle i_{Dr}\rangle}{\partial T_{on}} = \frac{V_{in}^2}{2L_m(V_{\mathrm{LED}1} + V_{\mathrm{LED}2})} \tag{13}$$

$$\frac{\partial\langle i_{Dr}\rangle}{\partial V_{\mathrm{LED}1}} = \frac{\partial\langle i_{Dr}\rangle}{\partial V_{\mathrm{LED}2}} = -\frac{V_{in}^2\,T_{on}}{2L_m(V_{\mathrm{LED}1} + V_{\mathrm{LED}2})^2}. \tag{14}$$

Now, the control-to-output transfer functions of $V_{\mathrm{LED}1}$ and $V_{\mathrm{LED}2}$, the proposed driver can be obtained with $\langle i_{Dr}\rangle$ and Z_1, where Z_1 is the impedance of the parallel-connected C_{o1} and $R_{\mathrm{LED}1}$($Z_1 = R_{\mathrm{LED}1}/(1 + sC_{o1}R_{\mathrm{LED}1})$) as follows:

$$\begin{aligned}\partial V_{\mathrm{LED}1} &= \partial\langle i_{Dr}\rangle Z_1 \\ &= Z_1\left(\frac{\partial\langle i_{Dr}\rangle}{\partial T_{\mathrm{on}}}\partial T_{\mathrm{on}} + \frac{\partial\langle i_{Dr}\rangle}{\partial V_{\mathrm{LED}1}}\partial V_{\mathrm{LED}1}\right)\end{aligned} \tag{15}$$

$$G_{v1c}(s) = \frac{\partial V_{\mathrm{LED}1}}{\partial T_{\mathrm{on}}} = \frac{\frac{\partial\langle i_{Dr}\rangle}{\partial T_{\mathrm{on}}}Z_1}{1 - \frac{\partial\langle i_{Dr}\rangle}{\partial V_{\mathrm{LED}1}}Z_1}. \tag{16}$$

Then, the control to output transfer function of $V_{\mathrm{LED}1}$ can be rearranged as follows:

$$G_{v1c}(s) = \frac{G_{01}}{1 + \frac{s}{\omega_p}} \tag{17}$$

$$G_{01} = \frac{V_{\mathrm{in}}^2 R_{\mathrm{LED}1}(V_{\mathrm{LED}1} + V_{\mathrm{LED}2})}{2L_m(V_{\mathrm{LED}1} + V_{\mathrm{LED}2})^2 + V_{\mathrm{in}}^2 T_{\mathrm{on}} R_{\mathrm{LED}1}} \tag{18}$$

$$\omega_p = \frac{1}{C_{o2}R_{\mathrm{LED}1}} + \frac{V_{\mathrm{in}}^2 T_{\mathrm{on}} R_{\mathrm{LED}1}}{2L_m C_{o1} R_{\mathrm{LED}1}(V_{\mathrm{LED}1} + V_{\mathrm{LED}2})^2}. \tag{19}$$

From (18), it can be noted that the control-to-output transfer function of the proposed driver is a one-pole system. Also, the control to output transfer function of $V_{\mathrm{LED}2}$ can be obtained in a similar way from the following:

$$\begin{aligned}\partial V_{\mathrm{LED}2} &= \partial\langle i_{Dr}\rangle Z_2 \\ &= Z_2\left(\frac{\partial\langle i_{Dr}\rangle}{\partial T_{\mathrm{on}}}\partial T_{\mathrm{on}} + \frac{\partial\langle i_{Dr}\rangle}{\partial V_{\mathrm{LED}2}}\partial V_{\mathrm{LED}2}\right).\end{aligned} \tag{20}$$

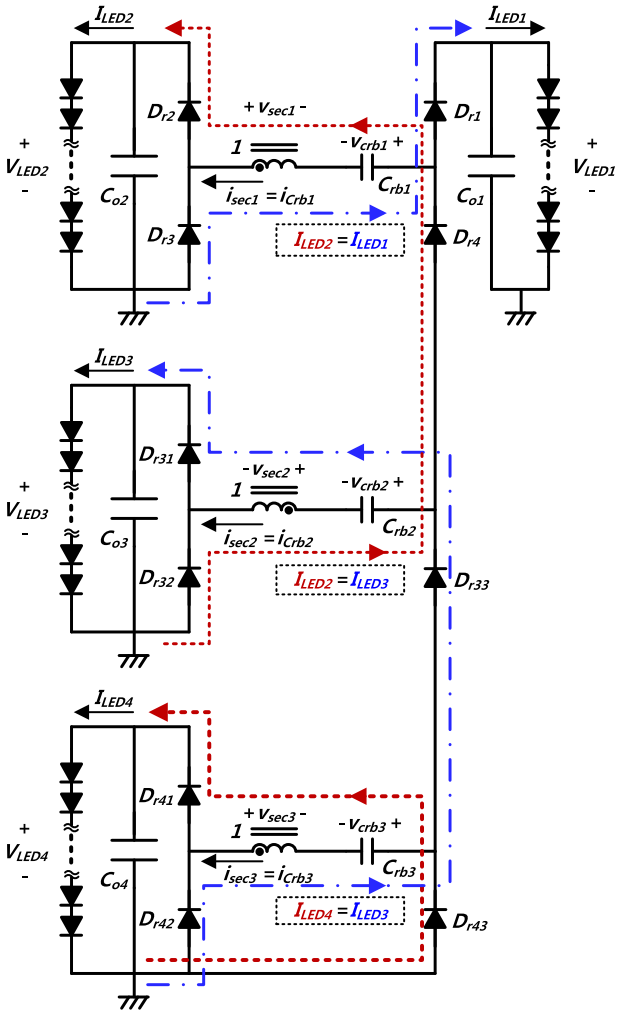

Fig. 7. Extension to the multioutput structure with capacitive balancing [11].

The control-to-output-current of LED1 can be obtained as $G_{v1c}(s)$ divided by the resistance of a LED string $G_{i1c}(s) = G_{v1c}(s)/R_{\mathrm{LED1}}$. In a similar way, $G_{i2c}(s) = G_{v2c}(s)/R_{\mathrm{LED2}}$. Then, at a high frequency much higher than the pole of the system, where the stability issue is directly related, the total control-to-output-current of the proposed driver can be obtained as follows:

$$G_{ic}(s) = G_{i1c}(s) + G_{i2c}(s) \cong \frac{1}{s}\left(\frac{G_{01}\omega_{p1}}{R_{\mathrm{LED1}}} + \frac{G_{02}\omega_{p2}}{R_{\mathrm{LED2}}}\right). \tag{21}$$

D. Extension to a Multichannel LED Driver

Because a capacitive balancing method has a very simple structure, present study already has extended it to a multioutput structure. A representative study about the extension is provided in [11]. In order to apply the capacitive balancing to the multioutput structure, the study used a series–parallel rectifier with blocking capacitors. In the proposed driver, the extension can be achieved by replacing the blocking capacitors with the resonant-blocking capacitors, as shown in Fig. 7. In this structure, $I_{\mathrm{LED}k}$ and $I_{\mathrm{LED}k+1}$ flows in the opposite direction through C_{rbk}, where $k = 1, 2$, and 3. Therefore, all currents in each LED string become naturally balanced. All resonant-blocking capacitors have the same capacitance C_{rb}.

In the proposed driver, the secondary-side currents flow following the dotted line in Fig. 7, when the main switch is turned ON. Also, the voltage across the secondary side of the transformer becomes V_{in}/n. Applying Kirchhoff voltage law (KVL) along the dotted lines results in the following:

$$\mathrm{Avg}(v_{cr4}) = \frac{V_{\mathrm{in}}}{n} - V_{\mathrm{LED4}} \tag{22}$$

$$\mathrm{Avg}\left(v_{crb2}\right) - \mathrm{Avg}\left(v_{crb3}\right) = -V_{\mathrm{LED2}} + \frac{2V_{\mathrm{in}}}{n}. \tag{23}$$

When the main switch is turned OFF, the secondary-side currents flow following the solid-dotted line in Fig. 7. Assuming $v_{\mathrm{sec1}} = v_{\mathrm{sec2}} = v_{\mathrm{sec3}} = v_{\mathrm{sec}}$, applying KVL along the solid-dotted line results in the following:

$$v_{\mathrm{sec}} = -\mathrm{Avg}(v_{cr2}) + V_{\mathrm{LED1}} \tag{24}$$

$$2v_{\mathrm{sec}} = -\mathrm{Avg}\left(v_{crb4}\right) + \mathrm{Avg}\left(v_{crb3}\right) + V_{\mathrm{LED3}}. \tag{25}$$

Combining (22)–(25) lead to the average voltage of all balancing capacitors as follows:

$$\mathrm{Avg}(v_{cr1}) = \frac{2V_{\mathrm{LED1}} - V_{\mathrm{LED2}} - V_{\mathrm{LED3}} - V_{\mathrm{LED4}}}{3} + \frac{V_{\mathrm{in}}}{n} \tag{26}$$

$$\mathrm{Avg}(v_{cr2}) = \frac{2V_{\mathrm{LED1}} + 2V_{\mathrm{LED2}} - V_{\mathrm{LED3}} - V_{\mathrm{LED4}}}{3} - \frac{V_{\mathrm{in}}}{n} \tag{27}$$

$$\mathrm{Avg}(v_{cr3}) = \frac{V_{\mathrm{in}}}{n} - V_{\mathrm{LED4}}. \tag{28}$$

The effective resonant capacitance (C_{rb_eff}) in the multioutput structure can be determined by the simplified equivalent circuit for C_{rb_eff}, as shown in Fig. 8. When the main switch is turned ON, C_{rb1} and C_{rb2} are series connected with two secondary windings, and C_{rb3} is series connected with one secondary windings. From the figure, the reflected equivalent capacitance to the primary side of the proposed driver can be determined as $3C_{rb}/n^2$ so that the resonant period can be considered during the design. Further design of the proposed driver with the multioutput structure is omitted because of similarity with the two-channel structure and the space limitation of this paper.

III. Design Procedure

In order to verify the effectiveness of the proposed driver, 400-V input 150–100-V/0.3-A two-channel output prototype has been designed.

A. Turns Ratio of the Transformer and the Main Switch Selection

From the volt–sec balance condition in (4), it can be noted that $V_{\mathrm{LED1}} + \mathrm{Avg}(v_{crb})$ should be larger than zero, in order to

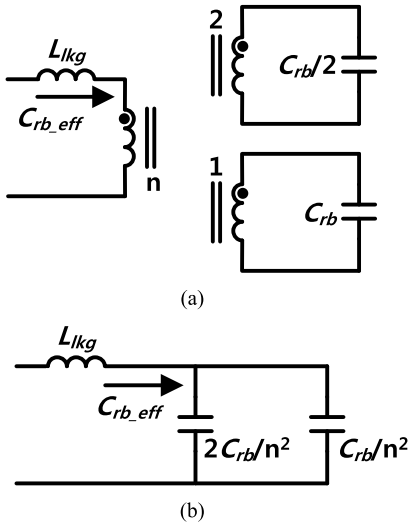

Fig. 8. (a) Simplified and (b) reflected C_{rb_eff} with a four-channel structure in Fig. 7.

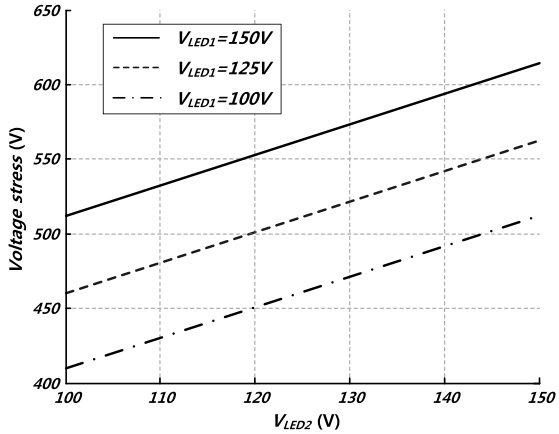

Fig. 9. Voltage stress on the main switch according to the different LED output voltages when $n = 2.05$.

reset i_{Lm}. By substituting (5) into (4), the required minimum turns ratio of the proposed driver can be obtained as follows:

$$V_{\mathrm{LED1}} + \mathrm{Avg}\,(v_{crb}) = V_{\mathrm{LED1}} + V_{\mathrm{LED2}} - V_{\mathrm{in}}/n > 0. \quad (29)$$

Because V_{LED1} and V_{LED2} vary according to its operating temperature, $\mathrm{Avg}(v_{crb})$ should make $V_{\mathrm{LED1}} + V_{\mathrm{LED2}} + \mathrm{Avg}(v_{crb})$ larger than zero when $V_{\mathrm{LED1}} + V_{\mathrm{LED2}}$ is the minimum as follows:

$$V_{\mathrm{LED1\_min}} + V_{\mathrm{LED2\_min}} - V_{\mathrm{in}}/n > 0 \quad (30)$$

where $V_{\mathrm{LED1\_min}}$ and $V_{\mathrm{LED2\_min}}$ are the minimum values of V_{LED1} and V_{LED2}, respectively. Rearranging (30) allows obtaining the minimum turns ratio of the proposed driver as follows:

$$n > V_{\mathrm{in}}/\left(V_{\mathrm{LED1\_min}} + V_{\mathrm{LED2\_min}}\right). \quad (31)$$

The voltage stress on the main switch, when the main switch is turned OFF, can be obtained by $V_{\mathrm{in}} + n(V_{\mathrm{LED1}} + \mathrm{Avg}(v_{crb}))$, and it is maximum when V_{LED1} and V_{LED2} are maximum as follows:

$$v_{ds\_\max} = n(V_{\mathrm{LED1\_max}} + V_{\mathrm{LED2\_max}}). \quad (32)$$

From (31) and (32), it can be noted that wide output voltage range makes *n* larger, resulting in large voltage stress on the main switch in the proposed driver. However, it only requires high-voltage-rated switch, not additional components like the case of the LLC converter. According to (31), *n* should be larger than $400/(100 + 100) = 2$.

With the given minimum *n*, the selection of turns ratio in the primary-side inverter is directly related to the selection of the main switch. With a larger *n*, the RMS current on the main switch can be reduced. However, the turn-on resistance becomes larger with larger *n* because the voltage stress on the main switch becomes larger. For these reasons, the selection of the main switch can be different according to the designers' choice.

With given main switch, a large *n* reduces RMS current in the primary side. However, a large *n* results in a high-voltage stress on the main switch causing a reduced margin on the voltage stress. With larger *n*, therefore, a snubber resistance, which determines the peak voltage stress, should be small enough to clamp the peak voltage stress at a safe level. Therefore, it can be noted that there is a tradeoff between conduction and snubber losses in the forward-flyback inverter. Considering the tradeoff, $n = 78:38 = 2.05$ is selected in this example. Although *n* is slightly larger than the required value, the ripple of v_{crb} makes sure that i_{Lm} can be reset because v_{crb} increases when the main switch is turned OFF. Also, the maximum voltage stress on the main switch becomes $2.05(150 + 150) = 615$ V, as shown in Fig. 9, so that the selection of 800-V-rated switch as the main switch is reasonable, considering the peak voltage stress on the main switch becomes $V_{\mathrm{in}} + V_{\mathrm{snb}}$.

B. Transformer Core, Magnetizing Inductance, and Switching Frequency

The selection of the transformer core is usually conducted according to the area product (A_p), which is the product of the window area and the cross-sectional area of the transformer core. In the proposed driver, A_p value of the transformer core can be deduced as follows:

$$A_p = \frac{V_{\mathrm{in}} T_{\mathrm{on}}}{B_{\max} K_u J}\left(i_{\mathrm{pri\_RMS}} + \frac{i_{\mathrm{sec\_RMS}}}{n}\right) \quad (33)$$

where V_{in}, T_{on}, $B_{\max}$, K_u, J, $i_{\mathrm{pri\_RMS}}$, $i_{\mathrm{sec\_RMS}}$, and *n* are the input voltage, on-time of the main switch, the maximum flux density of the transformer core, the window utilization factor, the current density of wires, the RMS current in the primary and secondary side, and the turns ratio of the transformer, respectively. Substituting (10) into (33) explains the relationship between L_m and A_p as follows:

$$A_p = \frac{2I_{\mathrm{LED}}\left(V_{\mathrm{LED1}} + V_{\mathrm{LED2}}\right)}{B_{\max} K_u J V_{\mathrm{in}}} \times \left(i_{\mathrm{pri\_RMS}} + \frac{i_{\mathrm{sec\_RMS}}}{n}\right) \times L_m. \quad (34)$$

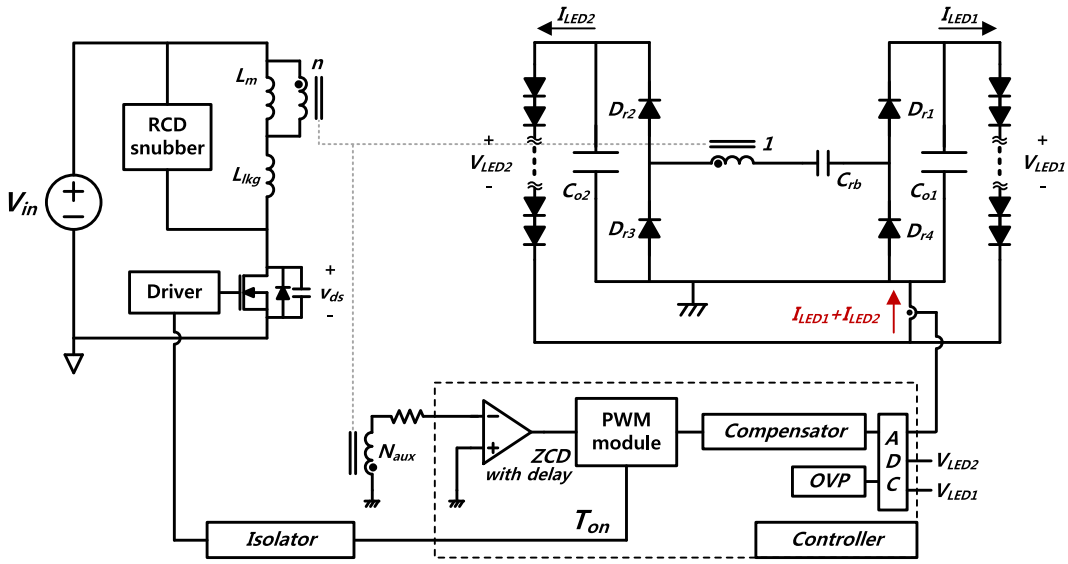

Fig. 10. Current control strategy for the proposed driver.

As shown in (34), the size of the transformer core is directly proportional to L_m, which is proportional to the switching period according to (7) and (10). Therefore, a higher switching frequency results in a smaller size of the transformer resulting in a reduced transformer loss. However, a higher switching frequency results in a large switching loss. For these reasons, the tradeoff between transformer size and switching loss should be considered during the transformer core selection.

C. Resonant Tank Design

The proposed driver can operate at a below resonant region in the entire load condition, when C_{rb} is smaller so that it almost removes the reverse recovery losses of the rectifier diodes. However, the conduction loss can be increased when C_{rb} is too small because RMS current of the driver is increased. Therefore, when C_{rb} is small enough to make the proposed driver operate in a below region, the efficiency when $V_{\mathrm{LED1}} = V_{\mathrm{LED2}} = 100$ V can be improved. On the other hand, the efficiency when $V_{\mathrm{LED1}} = V_{\mathrm{LED2}} = 150$ V would be lower than the prototype because conduction losses can be increased.

In the prototype, the authors aimed to obtain the maximum efficiency when the output power is the maximum. Therefore, the prototype operates in a below region when $V_{\mathrm{LED1}} = V_{\mathrm{LED2}} = 150$ V and in slightly above region when $V_{\mathrm{LED1}} = V_{\mathrm{LED2}} = 100$ V. The maximum T_{on} ($T_{\mathrm{on\_max}}$) occurs when $V_{\mathrm{LED1}} = V_{\mathrm{LED2}} = 150$ V, and its minimum ($T_{\mathrm{on\_min}}$) occurs when $V_{\mathrm{LED1}} = V_{\mathrm{LED2}} = 100$ V. In order for the proposed driver to operate in a below/above resonant region when the output power is maximum/minimum, a half of the resonant period should be located between $T_{\mathrm{on\_min}}$ and $T_{\mathrm{on\_max}}$. With given n, L_{lkg}, $T_{\mathrm{on\_min}}$, and $T_{\mathrm{on\_max}}$, C_{rb} can be chosen considering the duration of mode 1 as follows:

$$T_{\mathrm{on\_min}} < \pi\sqrt{L_{\mathrm{lkg}}C_{rb}}/n < T_{\mathrm{on\_max}} \tag{35}$$

$$(nT_{\mathrm{on\_min}}/\pi)^2/L_{\mathrm{lkg}} < C_{rb} < (nT_{\mathrm{on\_max}}/\pi)^2/L_{\mathrm{lkg}}. \tag{36}$$

D. Voltage Stress on Rectifier Diodes

The voltage stress on rectifier diodes in the proposed driver is clamped to the voltage sources related to the output voltage. The voltage stress on rectifier diodes with full-bridge type rectifier is determined by the output voltage as follows:

$$V_{Dr1\_\max} = V_{Dr4\_\max} = V_{\mathrm{LED1}} \tag{37}$$

$$V_{Dr2\_\max} = V_{Dr3\_\max} = V_{\mathrm{LED2}} \tag{38}$$

where $V_{Dr1\_\max}$, $V_{Dr2\_\max}$, $V_{Dr3\_\max}$, and $V_{Dr4\_\max}$ represent the maximum voltage stress on the rectifier diodes D_{r1}, D_{r2}, D_{r3}, and D_{r4}, respectively.

Also, the voltage stress on rectifier diodes with voltage-doubler-type rectifier is determined by the sum of the output voltages as follows:

$$V_{Dr1\_\max} = V_{Dr2\_\max} = V_{\mathrm{LED1}} + V_{\mathrm{LED2}}. \tag{39}$$

It should be noted that the proposed driver has a clamped-voltage stress on the rectifier diodes so that it is possible to use a low-voltage-rated diodes, as compared to the flyback driver with CST.

IV. Implementation and Experimental Results

A. Implementation of the Proposed Driver

Fig. 10 shows the control strategy of the proposed driver. Because I_{LED1} and I_{LED2} are balanced inherently, the sum of them is controlled. On-time information at the output of compensator is transferred to the primary side of the driver using photocoupler so that the output current can be controlled by the on-time of the main switch.

In order to make L_m operate with BCM, the zero current detection (ZCD) of L_m is required. ZCD can be implemented using auxiliary windings in the main transformer. After the current of L_m becomes zero, the voltage across it varies by the resonance between L_m and the output capacitor of the main

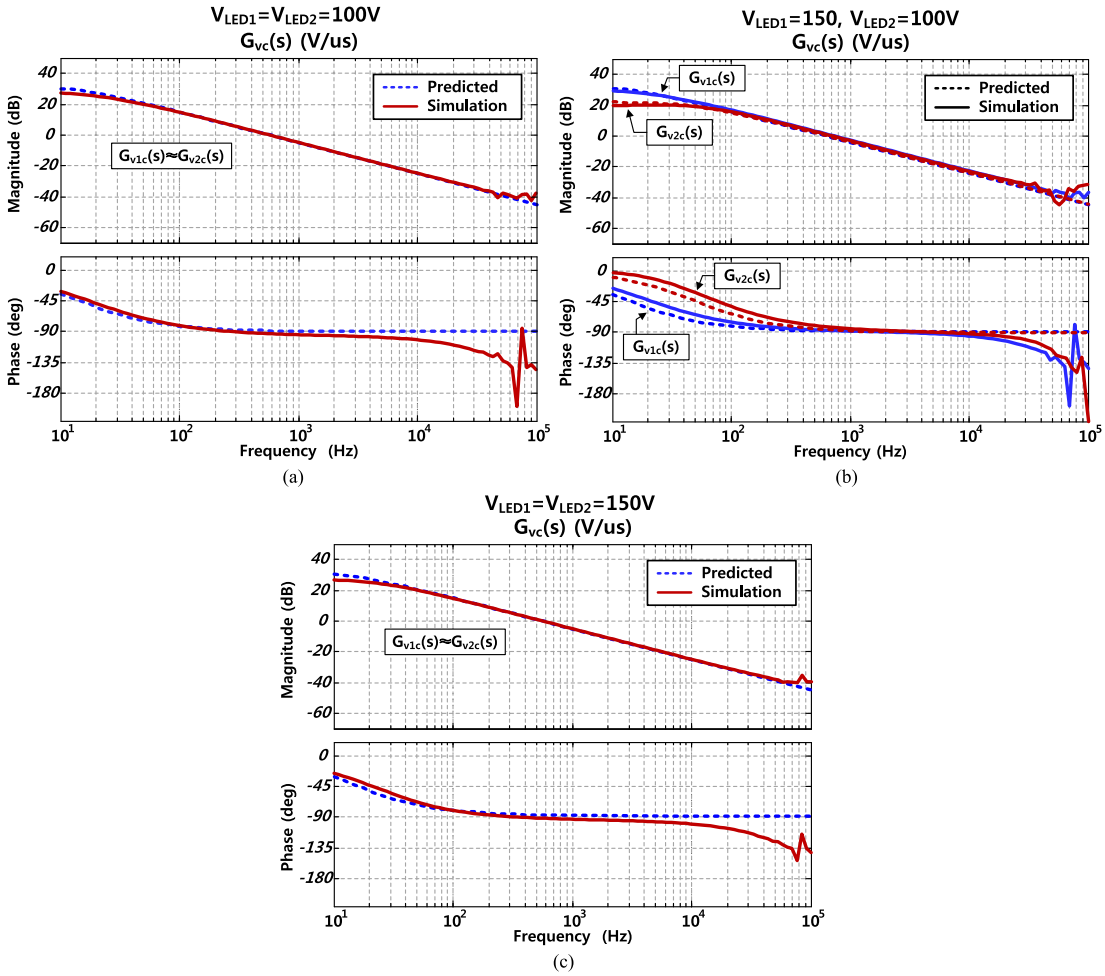

Fig. 11. Comparison between (18) and the simulation results when (a) $V_{\mathrm{LED1}} = V_{\mathrm{LED2}} = 100$ V (b) $V_{\mathrm{LED1}} = 150$ V, $V_{\mathrm{LED2}} = 100$ V, (c) $V_{\mathrm{LED1}} = V_{\mathrm{LED2}} = 150$ V.

switch. An analog comparator detects the voltage across L_m, and the PWM module turns-on the main switch at the rising edge of the output of the comparator. Some delay is required so that the main switch is turned ON when the voltage across it is the minimum. This ZCD scheme is widely used in many CRM flyback converters because of its simplicity. A digital controller TMS320F28069PZT is used in this example because of the design flexibility of the digital control.

According to the previous analysis, components for the prototype are selected with a full-bridge-type rectifier: $n:1 = 78:38$, $L_m = 1.5$ mH, and $L_{\mathrm{lkg}} = 8$ μH with RM8 transformer core, 250-V/220-nF capacitor for C_{rb}, FQP6N80 for the main switch, MBRB40250TG for the rectifier diodes, 10-nF miler capacitor, and 100-kΩ resistor for the RCD snubber.

The control-to-output transfer function has been verified by the simulation results with PSIM. From Fig. 11, it can be noted that the control-to-output transfer function of the proposed driver is quite exact, compared to the simulation results. Because the cutoff frequency of the closed-loop system is usually set from 1 to 10 kHz, the small-signal model provided in this paper can be effectively used for designing compensators.

In order to satisfy the stability of the one-pole system, PI or type 2 controllers can be used for the proposed driver. Because of the space limitation of this paper, further details are omitted.

B. Experimental Results

Figs. 12(a) and 13(a) show the experimental waveforms when $V_{\mathrm{LED1}} = V_{\mathrm{LED2}} = 150$ V. It is shown that the current of each LED is precisely balanced due to the charge balance of C_{rb}. The valley switching technique reduces the switching loss. The reverse recovery loss of the rectifier diodes is minimized because of soft switching

Figs. 12(b) and 13(b) show the experimental waveforms when $V_{\mathrm{LED1}} = V_{\mathrm{LED2}} = 100$ V. Similar with the conventional BCM flyback converter, T_{on} and the switching frequency are decreased since the output power decreased. Although the driver operating in an above resonant region causes the reverse recovery losses of the rectifier diodes, the efficiency is not severely degraded because the switching frequency is decreased.

Therefore, the proposed driver with a full-bridge-type rectifier shows a high efficiency of 96.2% and 94.1% when $V_{\mathrm{LED1}} = V_{\mathrm{LED2}} = 150$ V and $V_{\mathrm{LED1}} = V_{\mathrm{LED2}} = 100$ V, respectively. The proposed driver with a voltage-doubler-type rectifier can achieve higher efficiency because the number of rectifier diode can be reduced. Also, more optimized design considering the tradeoffs mentioned in this paper (L_m, f_s and A_p, n, and $v_{ds\_\max}$) in the proposed driver can lead to a higher efficiency. The current balancing characteristic is conserved due

TABLE I
COMPARATIVE COMPONENT SELECTION FOR LLC WITH BLOCKING CAPACITOR [9] AND THE PROPOSED DRIVER (PRICES FOR MAGNETIC AND THE OTHER COMPONENTS ARE FROM ALIEXPRESS.COM AND DIGIKEY.COM, RESPECTIVELY)

Components	LLC driver in [9]		Proposed driver with full bridge rectifier	
	Design result	Price (in USD)	Design result	Price (in USD)
Transformer	RM8 (63:35) $L_m = 700\ \mu$H, $L_{\rm lkg} = 5.6\ \mu$H	1.84	RM8 (78:38) $L_m = 1.5$ mH, $L_{\rm lkg} = 8\ \mu$H	1.84
Resonant inductor	RM6 (180 μH)	1.18	–	–
Main swtich(es)	FQPF5N50 2EA (500 V, 5 A, 1.4 Ω)	2.1	FQP6N80 1EA (800 V, 5.5 A, 2.5 Ω)	1.57
Blocking capacitor	B32522C1105K289 (100 V, 1 μF, 945 mm^3)	0.43	B32522C324J289 (250 V, 220 nF, 945 mm^3)	0.27
Total	Two magnetic cores 1-μF capacitor Two switches	5.55	One magnetic core 220-nF capacitor One switch	3.68

TABLE II
COMPARATIVE COMPONENT SELECTION FOR FLYBACK WITH CST [3] AND THE PROPOSED DRIVER (PRICES FOR MAGNETIC AND THE OTHER COMPONENTS ARE FROM ALIEXPRESS.COM AND DIGIKEY.COM, RESPECTIVELY)

Components	Flyback driver in [3]		Proposed driver with voltage doubler rectifier	
	Design result	Price (in USD)	Design result	Price (in USD)
CST	RM6 (1745 mm^3)	1.18	–	–
Blocking capacitor	–	–	B32522C324J289 (250 V, 220 nF, 945 mm^3)	0.27
Rectifier diodes	US1 K 2 EA (800 V, 1 A, 1.7 V_F)	0.88	US1G (400 V, 1 A, 1.4 V_F)	0.88
Total	One magnetic core Two diodes	2.06	One capacitor Two diodes	1.15

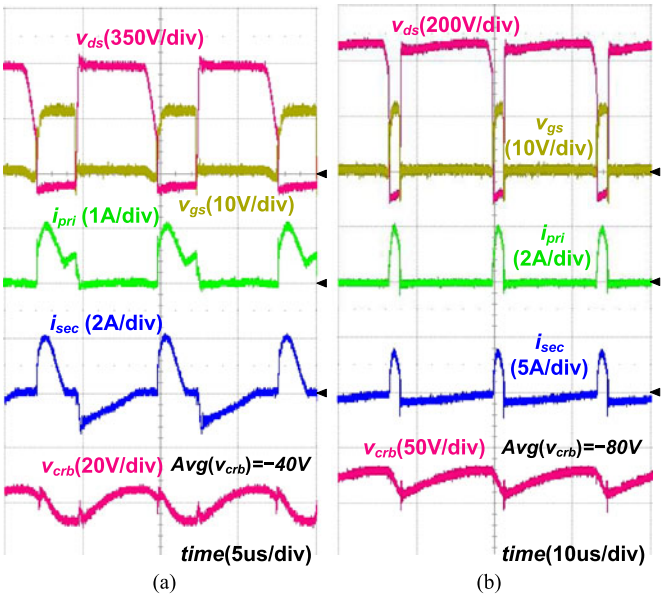

Fig. 12. Key waveforms of the proposed driver when (a) $V_{\rm LED1} = V_{\rm LED2} = 150$ V and (b) $V_{\rm LED1} = V_{\rm LED2} = 100$ V.

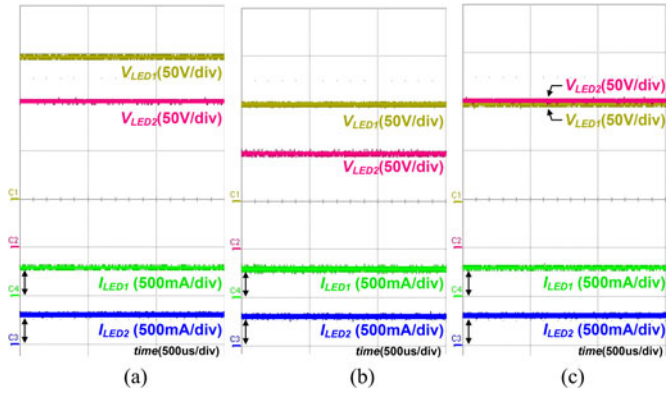

Fig. 13. Balanced currents of the proposed driver when (a) $V_{\rm LED1} = V_{\rm LED2} = 150$ V, (b) $V_{\rm LED1} = V_{\rm LED2} = 100$ V, and (c) $V_{\rm LED1} = 100$ V and $V_{\rm LED2} = 150$ V.

to C_{rb} although the LED voltages are different, as shown in Fig. 13(c).

C. Price and Power Density Comparison With Conventional Drivers

Table I shows the main components and price comparison between the LLC [9] and the proposed driver with a full-bridge-type rectifier. As shown in the table, the LLC driver in [9] uses two magnetic cores, 1-μF capacitor, and two main switches, whereas the proposed driver uses only one magnetic core, 220-nF capacitor, and one main switch. As shown in Table I, the proposed driver reduces one magnetic core and one switch, compared to the LLC driver in [9]. In addition, although the proposed driver has higher voltage stress on the blocking capacitor, the size of the capacitor is the same with the LLC driver. Furthermore, the price of the capacitor is cheaper because its capacitance is much smaller than that of the LLC driver. Therefore, from the price comparison in Table I, it can be evidently shown that the proposed driver greatly reduces the price of the system. Fig. 14 shows magnetic and switch components for power density comparison used in (a) LLC driver and (b) the proposed driver. A_p of the proposed driver is 3136 mm^4, whereas it is 4087.6 mm^4 in the LLC driver. In addition, the power density of the driver can be more reduced in the proposed driver because the proposed driver uses only one main switch.

Table II shows the secondary-side component selection for flyback with CST and the proposed driver. Flyback driver with CST [3] uses RM6 core (1745 mm^3), whereas the proposed

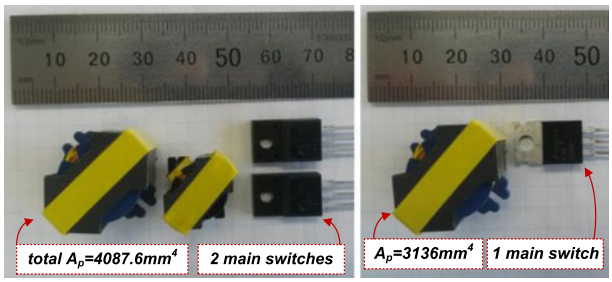

Fig. 14. Magnetic and switch components for power density comparison used in (a) LLC driver and (b) proposed driver.

driver uses resonant-blocking capacitor (945 mm^3), smaller than the CST. Also, the resonant-blocking capacitor is cheaper than CST so that the cost of the system can be reduced. Furthermore, the proposed driver uses lower-voltage-rated rectifier diodes with lower forward voltage drop so that the conduction losses can be more reduced. Due to removed core losses from CST and lower forward voltage drop of the rectifier diodes, it is evident that the proposed driver can have higher efficiency than the flyback driver.

V. Conclusion

In this paper, a single-switch forward-flyback two-channel LED driver is presented and analyzed. The equivalent power delivery model is derived so that the design of the proposed driver does not require much considering about the resonance. The proposed driver uses on-time controlled forward-flyback inverter in the primary side, and it uses resonant-blocking capacitor in the secondary side. It is possible for the proposed driver to obtain wide output voltage range and current balancing without any additional magnetic components so that the additional external inductor can be eliminated. Also, the proposed driver has much smaller voltage stress on the secondary rectifier diodes compared to the conventional flyback driver, allowing using low-voltage-rated diodes. Therefore, the proposed driver significantly reduces the cost of system and increases the power density with a high efficiency. Therefore, it can be a strong candidate for the two-channel LED applications.

References

[1] H. J. Chiu and S. J. Cheng, "LED backlight driving system for large-scale LCD panels," *IEEE Trans. Ind. Electron.*, vol. 54, no. 5, pp. 2751–2760, Oct. 2007.

[2] Y.-K. Lo, K.-H. Wu, K.-J. Pai, and H.-J. Chiu, "Design and implementation of RGB LED drivers for LCD backlight modules," *IEEE Trans. Ind. Electron.*, vol. 56, no. 12, pp. 4862–4871, Dec. 2009.

[3] X. Wu, Z. Wang, and J. Zhang, "Design considerations for dual-output quasi-resonant flyback LED driver with current-sharing transformer," *IEEE Trans. Power Electron.*, vol. 28, no. 10, pp. 4820–4830, Oct. 2013.

[4] R. Zhang and H. S. Chung, "Use of daisy-chained transformers for current-balancing multiple LED strings," *IEEE Trans. Power Electron.*, vol. 29, no. 3, pp. 1418–1433, Mar. 2014.

[5] W. Yu, J.-S. Lai, H. Ma, and C. Zheng, "High-efficiency dc–dc converter with twin bus for dimmable LED lighting," *IEEE Trans. Power Electron.*, vol. 26, no. 8, pp. 2095–2100, Aug. 2011.

[6] Y. Hu and M. M. Jovanovic, "A new current-balancing method for paralleled LED strings," in *Proc. IEEE 26th Annu. Appl. Power Electr. Conf.*, Mar. 2011, pp. 705–712.

[7] S. M. Baddela and D. S. Zinger, "Parallel connected LEDs operated at high frequency to improve current sharing," in *Proc. IEEE 39th Annu. Conf. Rec. Meeting Ind. Appl. Soc.*, Oct. 2004, vol. 3, pp. 1677–1681.

[8] J. Zhang, J. Wang, and X. Wu, "A capacitor-isolated LED driver with inherent current balance capability," *IEEE Trans. Ind. Electron.*, vol. 59, no. 4, pp. 1708–1716, Apr. 2012.

[9] X. Wu, J. Zhang, and Z. Qian, "A simple two-channel LED driver with automatic precise current sharing," *IEEE Trans. Ind. Electron.*, vol. 58, no. 10, pp. 4783–4788, Oct. 2011.

[10] J.-K. Kim, J.-B. Lee, and G.-W. Moon, "Isolated switch-mode current regulator with integrated two boost LED drivers," *IEEE Trans. Ind. Electron.*, vol. 61, no. 9, pp. 4649–4653, Sep. 2014.

[11] X. Wu, C. Hu, J. Zhang, and C. Zhao, "Series-parallel autoregulated charge-balancing rectifier for multioutput light-emitting diode driver," *IEEE Trans. Ind. Electron.*, vol. 58, no. 10, pp. 4783–4788, Oct. 2011.

[12] J. Zhang, L. Xu, X. Wu, and Z. Qian, "A precise passive current balancing method for multioutput LED drivers," *IEEE Trans. Power Electron.*, vol. 26, no. 8, pp. 2149–2159, Aug. 2011.

[13] C. Zhao, X. Xie, and S. Liu, "Multi-output LED drivers with precise passive current balancing," *IEEE Trans. Power Electron.*, vol. 28, no. 3, pp. 1438–1448, Mar. 2013.

[14] X. Wu, C. Hu, J. Zhang, and Z. Qian, "Analysis and design considerations of LLCC resonant multioutput DC/DC LED driver with charge balancing and exchanging of secondary series resonant capacitors," *IEEE Trans. Power Electron.*, vol. 30, no. 2, pp. 780–789, Feb. 2015.

[15] B. T. Irving, Y. Panov, and M. M. Jovanovic, "Small-signal model of variable-frequency Flyback converter," in *Proc. IEEE Appl. Power Electron. Conf.*, Feb. 2003, pp. 977–982.

Jong-Woo Kim (S'13) was born in Korea in 1987. He received the B.S. and M.S. degrees in electrical engineering from the Korea Advanced Institute of Science and Technology, Daejeon, Korea, in 2010 and 2012, respectively, where he is currently working toward the Ph.D. degree.

His research interests include dc–dc converter, power factor correction ac–dc converter, digital control, server power systems, and LED power system.

Jung-Pil Moon (S'15) was born in Korea in 1988. He received the B.S. degree in electrical and electronics engineering from Sungkyunkwan University, Suwon, Korea, in 2013, and the M.S. degree in electrical engineering from the Korea Advanced Institute of Science and Technology, Daejeon, Korea, in 2015.

He is currently working at Digital Media and Communications R&D Center, Samsung Electronics, Suwon. His research interests include dc–dc converter, power factor correction ac–dc converter, digital control, and wireless power transfer.

Gun-Woo Moon (S'92–M'00) received the M.S. and Ph.D. degrees in electrical engineering from the Korea Advanced Institute of Science and Technology (KAIST), Daejeon, Korea, in 1992 and 1996, respectively.

He is currently a Professor at the Department of Electrical Engineering, KAIST. His research interests include modeling, design and control of power converters, soft-switching power converters, resonant inverters, distributed power systems, power factor correction, electric drive systems, driver circuits of plasma display panels, and flexible ac transmission systems.

Dr. Moon is a Member of the Korean Institute of Power Electronics, the Korean Institute of Electrical Engineers, the Korea Institute of Telematics and Electronics, the Korea Institute of Illumination Electronics and Industrial Equipment, and the Society for Information Display.